Copper and nickel doping effect on interaction of SnO_2 films with H_2S

M. Rumyantseva,[a] M. Labeau,[b] G. Delabouglise,[b] L. Ryabova,[a] I. Kutsenok[a] and A. Gaskov*[a]

[a]*Chemistry Department of Moscow State University, 119899 Moscow, Russia*

[b]*Laboratoire des Materiaux et du Genie Physique, CNRS UMR 5628, Institut National Polytechnique de Grenoble, BP 46, 38402 Saint Martin d'Heres Cedex, France*

The pyrosol spraying deposition technique has been used for the synthesis of SnO_2, SnO_2–CuO and SnO_2–NiO polycrystalline films with grain size of 3–10 nm. The composition, microstructure and electrical properties of the films have been investigated by X-ray diffraction, electron probe microanalysis, Auger electron spectroscopy and X-ray photoelectron spectroscopy. The interaction of SnO_2, SnO_2–CuO and SnO_2–NiO polycrystalline films with the reducing gases: H_2S, C_2H_5OH, CO and CH_4 has been investigated by conductance measurements. It has been found that copper and nickel have a significant effect on the sensitivity of SnO_2 films to H_2S. The model of interaction of SnO_2 films with H_2S gas and different sensor properties of tin dioxide films doped with copper and nickel are discussed with regard to the position of these metals in the films.

Tin dioxide thin films and ceramics are widely used for gas sensor applications. The operation principle of such devices is based on the increasing of material conductance in the presence of reducing gases. For hydrogen sulfide this effect is related to an interaction of H_2S molecules[1] or its dissociation products[2] with O_2^- ions adsorbed on the SnO_2 grains. The effect of different doping metals on the response of SnO_2 materials to H_2S was analysed by Takahata.[3] It was suggested that some metal cations promote the H_2S dissociation to H^+, HS^- and S^{2-}. It was demonstrated that the cations with a low electronegativity value are best suited for SnO_2 doping with regard to hydrogen sulfide detection. However, it was found by Yamazoe and co-workers[4] that doping of tin dioxide ceramics with copper, that is intermediate in electronegativity, gives rise to the outstanding sensitivity $S=35\,000$ at 200 °C to 50 ppm H_2S in air. But in this case the mechanism of response is attributed to the chemical reaction of high-resistive CuO grains with H_2S. The formation of high conducting CuS results in removing of the electrical barrier between the n-SnO_2 and p-CuO grains. XPS analysis of Sn 3d, O 1s and S 2p electron transitions in air and H_2S containing atmosphere supports this supposition.[5] The extremely high sensitivity of SnO_2–CuO thin films and ceramics to H_2S was confirmed later.[6,7]

The importance of mutual reversible chemical transformations of corresponding oxides and sulfides in H_2S and air have been demonstrated. Recently we carried out the thermodynamic simulation of these chemical reactions for a variety of metals (M) by the Gibbs energy minimisation method[8] using the thermodynamic data bank IVTAN THERMO. The estimation of equilibrium composition for all binary phases in the system Sn–M–O–H–S was made under the experimental conditions: pure air or an atmosphere of 100 ppm of H_2S in air (temperature = 25–550 °C, pressure = 1 atm). It is demonstrated that Cu, Ni, Ag, Pb and Bi may by used for the development of SnO_2-based hydrogen sulfide gas sensors. Here we compare the composition, microstructure, electrical and sensing properties of SnO_2 thin films doped with two members of this group: copper and nickel. We examine the location of copper and nickel in SnO_2 polycrystalline thin films and their response to H_2S and other reducing gases.

Experimental

SnO_2, SnO_2–CuO and SnO_2–NiO thin films of 1.0–1.2 μm thickness were grown by pyrolysis of an aerosol generated by ultrahigh frequency. The synthesis process has been described in detail.[9] The precursors used were solutions of 0.2 M dibutyltin diacetate in acetylacetone, 0.05 M copper trifluoroacetylacetonate in butanol and nickel ethylhexanoate. The solutions were mixed to produce SnO_2 films with different copper and nickel contents. The concentrations of additive metals in the solution were: $[Cu]_{sol}=100[Cu]/([Cu]+[Sn])=0.0$, 0.1, 0.5, 1.0, 3.0 and 5.0%; $[Ni]_{sol}=100[Ni]/([Ni]+[Sn])=0.0$, 7.0, 23.0, 30.0, 38.0 and 57.0%. The films were deposited on oxidised ⟨100⟩ silicon at temperatures of 460, 490, 520 and 560 °C. The thickness of the SiO_2 layer was *ca.* 1.0 μm.

The films thickness and microstructure were studied by scanning electron microscopy (JSM-35, JEOL). X-Ray diffraction (XRD) patterns were obtained using a Siemens diffractometer with monochromatic Cu-Kα radiation. The SnO_2 average grain sizes depending on the synthesis conditions were calculated from the X-ray diffraction patterns using the Debye–Scherrer equation.

The copper and nickel concentrations in the films were determined by electron probe microanalysis (EPMA, Cameca-SX50). EPMA was performed for six points and four electron voltages: 8, 12, 16 and 20 kV. Single crystals of Si and SnO_2, ceramic Cu_2O and metallic Ni were used as reference samples. The mean values of the K ratio ($I_i/I_{i\ reference}$) of lines Si-Kα, Sn-Lα, Cu-Kα, Ni-Kα and O-Kα were determined for each sample and voltage. The results were treated using a multilayer analysis software based on the Pouchou and Pichoir model[10] of $\phi(\rho, z)$ function of depth distribution of ionisation.

Auger electron spectroscopy (AES) (JAMP-10, JEOL) was performed for six to eight points in vacuum (1×10^{-9} mmHg) with an electron energy of 3 keV and an electrical current of 1×10^{-8}–1×10^{-9} A. The primary electron beam diameter was 100 nm, and the points were spaced 500–1000 nm apart. The spectra were recorded from 50 to 1000 eV in the $dN(E)/dE$ mode. The copper and nickel oxidation states were analysed by X-ray photoelectron spectroscopy (XPS) using a PHI-5400 (Perkin Elmer) spectrometer with Mg-Kα radiation.

The samples conductance behaviour was investigated in the temperature range 77–273 K. Measurements were performed in dc regime at a fixed voltage $U=1$ V. The contact wires were carefully soldered on the preliminarily deposited gold layers. The current–voltage characteristics of the samples appear to be linear up to $U=10$ V.

The gas sensing properties, steady-state conductance and electrical response, were investigated in the temperature range 100–500 °C with an automatic measurement system in dry air, nitrogen and gas mixtures: (100–1200) ppm H_2S in nitrogen,

80 ppm ethanol in air, 300 ppm CO in air and 1000 ppm CH_4 in air. The contacts were pressed on thin gold films. Measurements of electric current which were proportional to the conductance were performed in dc mode at a fixed voltage $U=1$ V. The steady-state conductance is measured during the gradual temperature decrease from 500 to 100 °C. The comparison of the conductance values G_0 in dry air and G in the reducing gas containing atmosphere allowed the estimation of the film sensitivity $S=(G-G_0)/G_0$.

Results and Discussion

XRD demonstrates that all the obtained films were of the cassiterite SnO_2 phase. It should be noted that no copper or nickel containing phases were detected apparently owing to the low content of these phases in the films as well as their small dimensions. The widths of the SnO_2 lines in the diffractograms depended on the growing process temperature. The influence of synthesis conditions on the SnO_2 grain size is shown in Table 1. The value of the average grain size calculated from the Debye–Scherrer equation varies from 3.0 to 10.0 nm for the most of the layers. Larger crystallite sizes were obtained at a higher deposition temperature for a given content of added metal in the initial solution. The copper or nickel content in the solution has only a minor effect on the grain size.

Table 1 Copper and nickel content, SnO_2 average grain size and film resistance as a function of the deposition temperature (T) and concentration of the metal in the initial solution

T/°C	$[M]_{solution}$ (%)	$[M]_{film}$ (atom%)	SnO_2 average grain size/nm	R/Ω ($T=273$ K)
		SnO_2		
460	—	—	5.6	3×10^6
490			6.8	2.7×10^5
520			9.0	1.3×10^5
560			10.5	5.6×10^4
		SnO_2–CuO		
460	0.1	0.73	4.0	5.0×10^7
	0.5	1.26	3.9	1.4×10^8
	1.0	2.45	2.6	3.0×10^7
	3.0	2.50	3.6	1.2×10^7
490	0.1	0.52	6.5	2.9×10^7
	0.5	1.20	5.7	5.3×10^7
	1.0	1.45	5.0	1.9×10^8
	3.0	1.40	5.1	1.3×10^7
520	0.1	0.16	8.4	1.0×10^7
	0.5	0.76	6.3	1.4×10^7
	1.0	1.16	5.3	2.0×10^8
	3.0	1.58	7.0	1.5×10^7
560	0.1	0.09	10.3	1.5×10^7
	0.5	0.23	9.1	2.9×10^7
	1.0	0.66	6.8	2.8×10^7
	3.0	0.9	10.0	1.4×10^7
		SnO_2–NiO		
460	7.0	0.16	6.2	1.9×10^5
	23.0	0.36	5.7	
	30.0	0.78	4.5	1.38×10^7
	38.0	1.13	5.0	
	57.0	1.90	4.8	
490	7.0	0.16	7.0	3.5×10^5
	23.0	0.45	6.9	3×10^6
	30.0	0.89	5.6	5.6×10^6
	38.0	1.25	5.6	2×10^7
	57.0	2.83	6.1	6×10^6
520	7.0	0.21	7.8	1.9×10^6
	23.0	0.67	8.3	
	30.0	1.27	7.9	
	38.0	1.44	7.4	
	57.0	2.63	10.1	
560	7.0	0.28	9.9	1.2×10^5
	23.0	0.79	10.2	
	30.0	1.51	9.1	1.1×10^7
	38.0	1.52	11.6	
	57.0	1.53	17.1	

The microstructure studies demonstrate that the films have a porous structure and SnO_2 grains are combined into aggregates of 30–150 nm in diameter. The secondary electron micrograph of Fig. 1 was obtained on the cross-section of a SnO_2–CuO film deposited at 520 °C. The size of most of the aggregates is in the range 60–100 nm.

The content of copper and nickel in the films is listed in Table 1 as a function of the growth temperature and the composition of initial solution. The concentration of copper in the films increases from 0.1 up to 2.5 atom% with decreasing deposition temperature and increasing copper concentration in the initial solution. It is worth noting that SnO_2–CuO films prepared in this work have low copper concentrations in comparison with ceramic samples (SnO_2+5 mass% CuO) studied in ref. 4–6. The highest concentration of Cu of *ca.* 2.5 atom% was found in the film prepared at 460 °C from a solution containing 3.0% Cu. An increase of copper concentration to >5.0% results in precipitation in the initial solution. The maximum Ni concentration was 2.8 atom% at a deposition temperature of 490 °C and for a solution containing 57% Ni.

XPS analysis demonstrates that both Cu and Ni are likely to be divalent in the SnO_2 films. Small changes in the peak position of Cu $2p_{3/2}$ and Ni $2p_{3/2}$ from the binding energy corresponding to oxidation state (+2) is due to instability of Cu—O and Ni—O bonds under high vacuum conditions, as reported previously in ref. 11. XPS investigation of Sn $3d_{5/2}$ and O 1s levels shows that these binding energies are lower for the doped SnO_2 films compared with pure tin dioxide. Analysis of relative energy of Sn $3d_{5/2}$ (E_1) and O 1s (E_2) levels in the pure and doped films revealed that nickel even at a concentration as low as 1.2 atom% has a pronounced effect on the value of E_2–E_1 in SnO_2. The same concentration of copper in the films has no influence on the relative binding energy.

AES depth analysis of copper and nickel concentration also demonstrates the different behaviour of these doping metals in polycrystalline SnO_2 films. It was found that copper produces a segregation in the surface layer. In SnO_2 films doped with 1.5 atom% Cu the coefficient of copper distribution $K_{Cu}=[Cu]_s/[Cu]_d$ between the surface $[Cu]_s$ and at a depth of 100 nm $[Cu]_d$ is >5. By contrast, AES depth analysis of SnO_2 films doped with the same concentration of Ni shows homogeneous nickel distribution ($K_{Ni}\approx1$.)

The SnO_2 grain size and content of additive metals in the films have an influence on the electrical properties presented in Table 1. Fig. 2(*a*) and (*b*) show the values of relative resistance

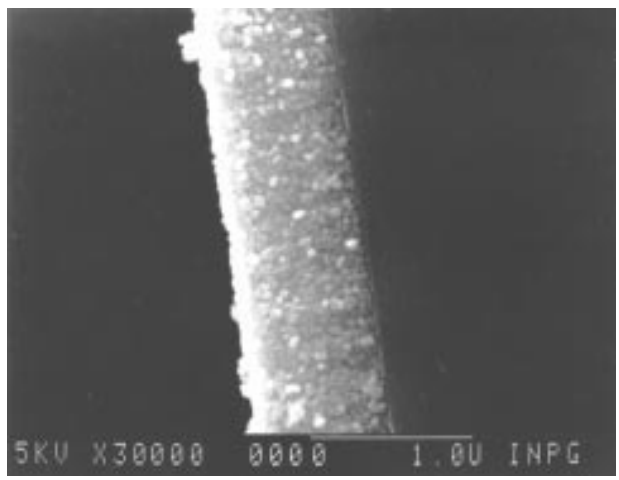

Fig. 1 Secondary electron micrograph of a SnO_2 film cross-section, typical thickness *ca.* 1 μm

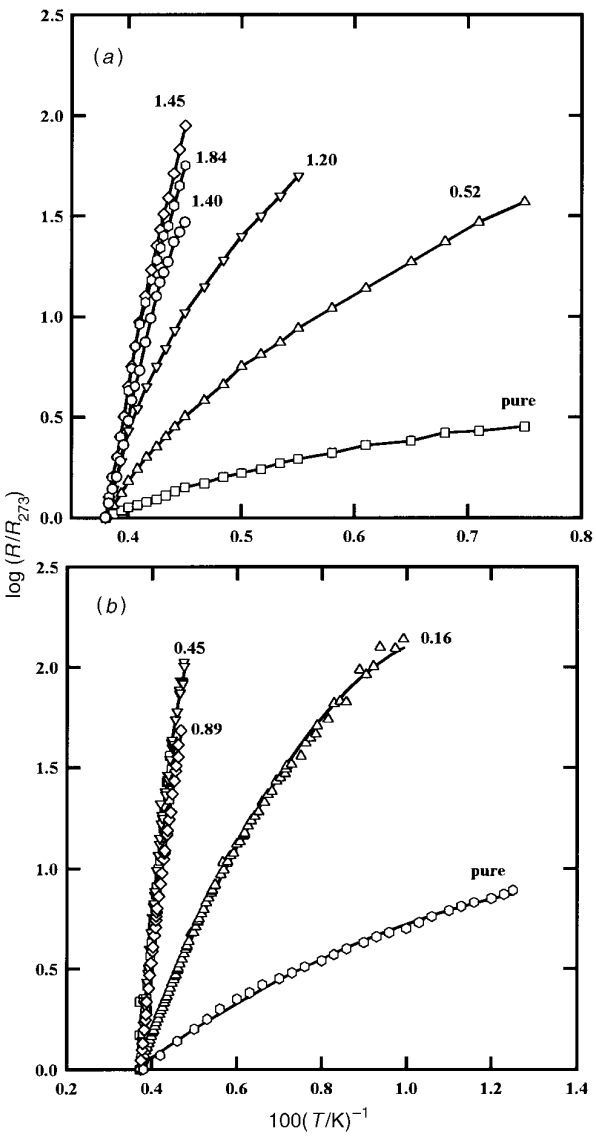

Fig. 2 Relative resistance as a function of temperature for SnO_2–CuO (*a*) and SnO_2–NiO (*b*) with different additive metal contents (in atom%)

$R_r = R(T)/R(T=273\ \mathrm{K})$ measured as a function of a temperature for series of SnO_2 films doped with copper [Fig. 2(*a*)] and nickel [Fig. 2(*b*)]. An increase of copper or nickel content results in growth of the samples' resistance accompanied by the appearance of a linear region on the curves of log R *vs.* $1/T$. The activation energy V calculated from the relation $R = \exp(V/kT)$ rises and saturates at a value of *ca.* 0.5 eV as copper and nickel concentration reach 1.0 and 0.45 atom%, respectively. The resistance character change seems to be connected with the acceptor action of both doping metals in SnO_2. The activation energy may be attributed to the barrier mechanism of conductivity in the investigated films. It is reasonable that the appearance of the barrier is connected with the effect of compensation of native donor oxygen vacancies V_O by acceptor impurities defects of substitution M_{Sn} in the tin dioxide structure. Processes on the grains boundaries, electrodes or substrate, may also contribute to barrier formation.

Steady-state conductance

Fig. 3–5 show the curves of steady-state conductance in air $G_0(T)$ and in the gas mixtures $G(T)$: 100 ppm H_2S+N_2, 80 ppm ethanol in air, 300 ppm CO in air and 1000 ppm CH_4

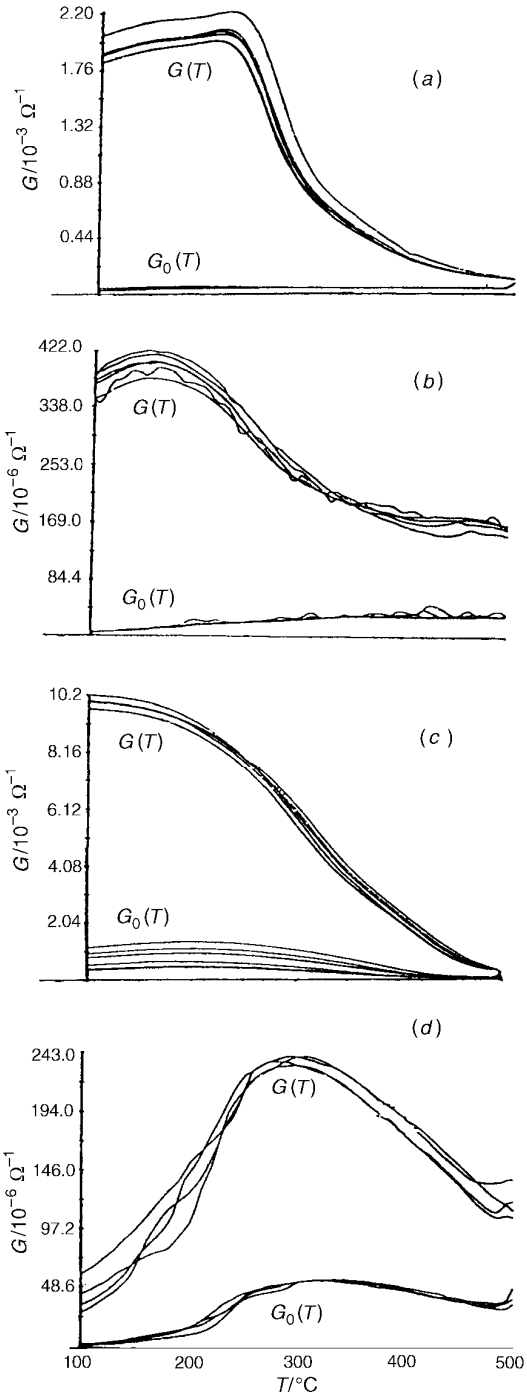

Fig. 3 Steady-state conductance curves for pure SnO_2, in air, $G_0(T)$, and in the gas mixture, $G(T)$: 80 ppm ethanol in air (*a*), 300 ppm CO in air (*b*), 100 ppm H_2S+N_2 (*c*) and 1000 ppm CH_4 in air (*d*)

in air for pure SnO_2 (Fig. 3), SnO_2–CuO films with 1.0 atom% Cu (Fig. 4) and SnO_2 films doped with 0.7 atom% Ni (Fig. 5). It can be seen that the shape of steady-state conductance curves measured in atmospheres containing H_2S and other reducing gas mixtures is significantly different from the G_0 curves. The curves $G_0(T)$ indicate semiconductor behaviour. The conductance in the presence of reducing gases is much higher than in the support gases (air, nitrogen). The $G(T)$ curves measured for the SnO_2–NiO films have a well defined maximum at 250 °C for C_2H_5OH, 210 °C for H_2S and 300 °C for CH_4. For SnO_2 doped with copper the $G(T)$ curves have a maximum only for C_2H_5OH at 210 °C, for other reducing

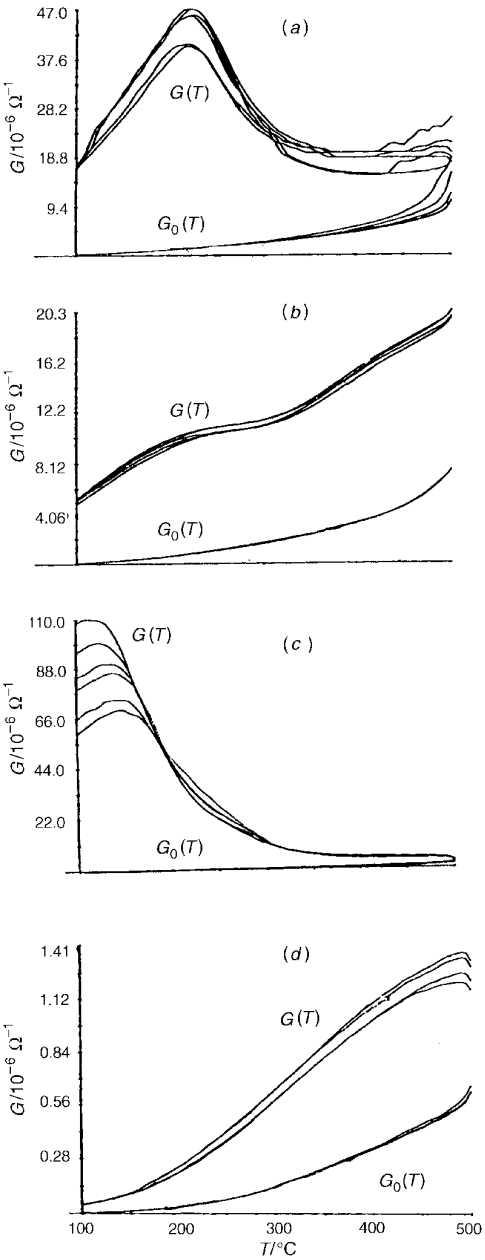

Fig. 4 Steady-state conductance curves for SnO_2–CuO films with 1.0 atom% Cu in air, $G_0(T)$, and in the gas mixture, $G(T)$: 80 ppm ethanol in air (*a*), 300 ppm CO in air (*b*), 100 ppm H_2S+N_2 (*c*) and 1000 ppm CH_4 in air (*d*)

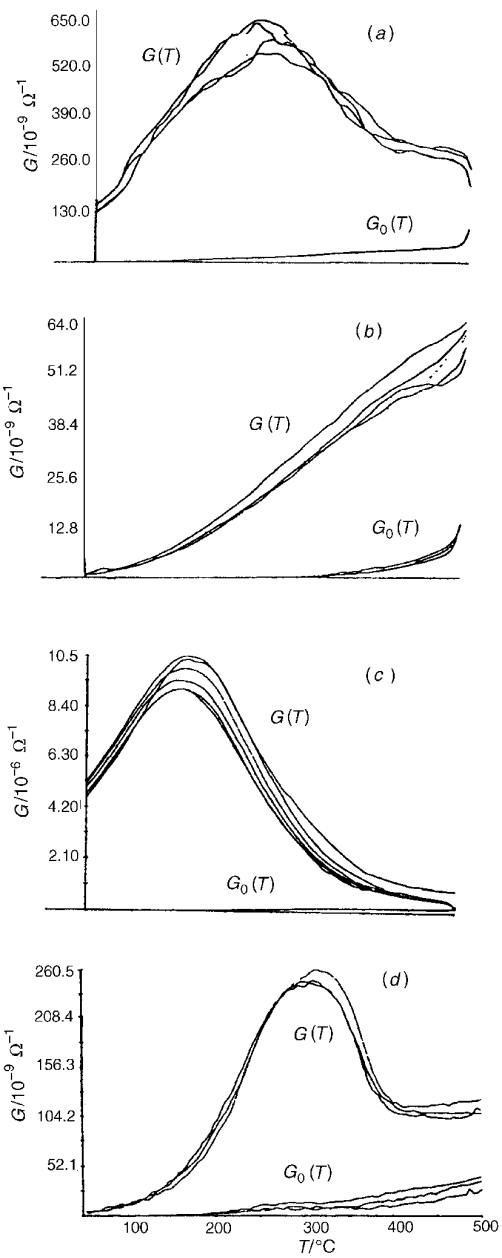

Fig. 5 Steady-state conductance curves for SnO_2–NiO films with 0.7 atom% Ni in air, $G_0(T)$, and in the gas mixture, $G(T)$: 80 ppm ethanol in air (*a*), 300 ppm CO in air (*b*), 100 ppm H_2S+N_2 (*c*) and 1000 ppm CH_4 in air (d)

gases studied in this work $G(T)$ curves are monotonous. The difference in the $G_0(T)$ and $G(T)$ curves provides a strong proof of the film sensitivity to the presence of reducing gases in the atmosphere. Copper and nickel exert a significant effect on steady-state conductance of the tin dioxide films. The essential difference of the doped films from pure SnO_2 is observed in the conductance–temperature dependences in air. For pure SnO_2 the value of G_0 at 100 °C varies in the range of $(0.2–5.0)\times10^{-4}$ Ω^{-1} depending on the growth conditions, while for doped samples containing 0.5–1.5 atom% of copper or nickel this value is 10^{-8}–10^{-9} Ω^{-1} (Table 1). Because of this difference films doped with copper and nickel are much more sensitive towards H_2S. For other reducing gases studied in this work no effect of copper and nickel on the gas sensitivity of SnO_2 films was found.

Electrical response

The electrical response is measured as a function of copper and nickel concentration and the operation temperature (T). The response transients on changing of the gas phase composition from air to 100 ppm H_2S in nitrogen at the temperature of 200 °C for the three films SnO_2, SnO_2–CuO and SnO_2–NiO is shown in Fig. 6. It should be noted that the rate of the film interaction with H_2S is rather slow. In H_2S containing atmospheres, the SnO_2 film reached a sensitivity $S=2–5$ in *ca.* 240 min. The relatively slow rate of response and recovery processes may be also caused by the inertness of our measurement cell. The resistance of SnO_2–CuO film in a 100 ppm H_2S containing atmosphere decreased by *ca.* 10^2–10^3 in 30 min. The maximum sensitivity values estimated from the electrical response for this film are 10^3–10^4 supporting the data of Yamazoe and co-workers.[4] On the other hand the rate of electrical response of

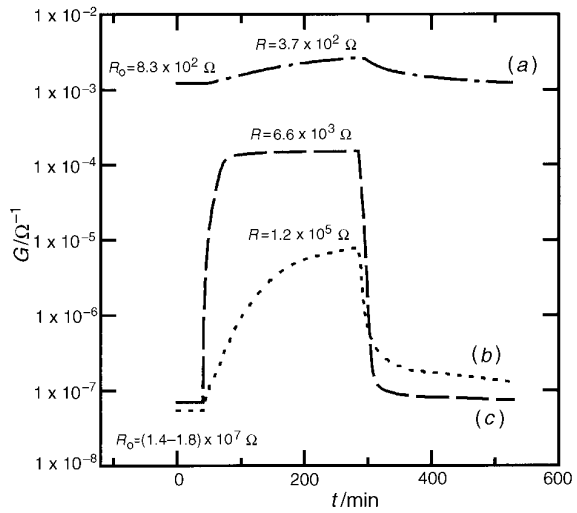

Fig. 6 Electrical response of (*a*) SnO_2, (*b*) SnO_2–CuO with 1.0 atom% Cu and (*c*) SnO_2–NiO with 0.7 atom% Ni films to 100 ppm H_2S in nitrogen at 200 °C

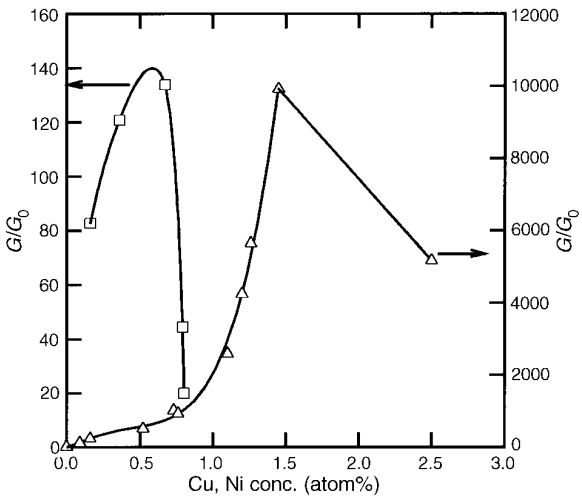

Fig. 7 SnO_2–CuO (△; 150 °C) and SnO_2–NiO (□; 250 °C) sensitivity to 100 ppm H_2S *vs.* copper and nickel concentration

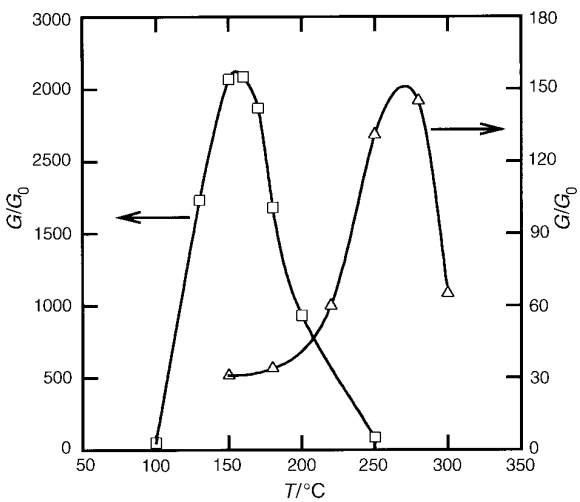

Fig. 8 Temperature dependence of sensitivity for 60 min of exposure in 100 ppm H_2S for SnO_2–CuO with 1.5 atom% Cu (□) and SnO_2–NiO with 0.7 atom% Ni (△)

SnO_2–NiO films is significantly slower. Although the sensitivity of these films in 100 ppm H_2S was comparable with that of SnO_2–CuO samples the time necessary to reach the steady-state conductance was >4 h.

It is interesting that for the doped films at 100–150 °C the full recovery time after removal of the test gas is greater than the response time taken to reach the saturation sensitivity value. However the rate of the removal process increases with operation temperature. At temperatures of 200–250 °C the resistance returns to the baseline in 15–20 min whereas the response time is considerably longer (70% of response time is *ca.* 40 min).

The sensitivity value of SnO_2 films to H_2S detection increases with copper and nickel content up to 1.5 and 0.7 atom% respectively as shown in Fig. 7. This is in accord with the electrical properties of the doped samples, the resistance of the films increasing similarly with copper and nickel concentration (Table 1). Fig. 8 shows the temperature dependence of sensitivity for the SnO_2 film doped with 1.1 atom% Cu and 0.7 atom% Ni for the same exposure time of 60 min in 100 ppm H_2S. The maximum of SnO_2–CuO film sensitivity $S=2500$ is attained at 150–160 °C. For SnO_2–NiO films the optimal conditions of gas response occur at 280 °C.

The sensitivity values for pure SnO_2, SnO_2–CuO and SnO_2–NiO films in H_2S (100 ppm)+N_2 are shown in Fig. 9 in comparison to the data obtained in the gas mixtures: 80 ppm C_2H_5OH in air, 300 ppm CO in air and 1000 ppm CH_4 in air. The results show the remarkable selectivity of the films doped with copper.

Despite some common properties of tin dioxide films doped with copper and nickel, the results obtained show evidence of some differences. (i) For SnO_2 films doped with nickel all the processes of solid–gas interaction are significantly slower than for SnO_2–CuO, leading to poorer response and recovery times. (ii) The temperature corresponding to the maximum of sensitivity for the SnO_2 films doped with nickel is higher than for SnO_2–CuO films.

The above features of SnO_2 films doped with copper and nickel may be explained by the difference in distribution of these metals between the surface and the bulk of the polycrystalline tin dioxide. It is suggested that most of the nickel atoms occupy tin positions in the tin dioxide structure forming acceptor centres Ni_{Sn}. By contrast, copper segregation on the surface is most likely with the Cu adding to polycrystalline

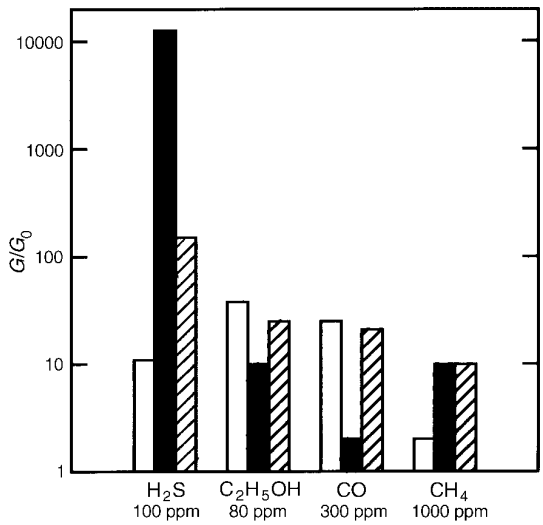

Fig. 9 Comparative sensitivity to different gases of the films: pure SnO_2 (white), SnO_2–CuO with 1.5 atom% Cu (black) and SnO_2–NiO with 0.7 atom% Ni (stripes) at a temperature of: 150 °C for H_2S, 250 °C for CO, 280 °C for C_2H_5OH and 300 °C for CH_4

SnO_2. Direct depth composition analysis by AES and indirect evidence obtained by XPS analysis of relative Sn—O binding energy in SnO_2–NiO and SnO_2–CuO films confirm these speculations.

Both Cu and Ni doping results in increased resistance. The concentration of native atomic defects $[V_O^{2+}]$ in tin dioxide varies in the range 10^{-2}–10^{-4} atom% as a function of $P(O_2)$ and temperature.[12] Formation in the bulk of SnO_2 doped with 0.7 atom% of nickel with a comparable concentration of acceptor centres $[Ni_{Sn}^{2-}]$ could give rise to the effect of compensation. For copper a calculation was performed on the p-CuO–n-SnO_2 junction influence on the conductance of SnO_2 films doped with 1.5 atom% Cu. It is known[13] that in a three-dimensional lattice the percolation mechanism occurs with a critical probability of occupation of sites from 0.50 up to 0.70. Assuming that copper forms a segregation layer of thickness 1 nm on the surface of the SnO_2 spherical particle, it can be shown that the limits of the percolation mechanism in tin dioxide films doped with 1.5 atom% Cu, may be achieved if the diameter of the SnO_2 particle is *ca.* 100 nm. It is reasonable to conclude that most of the copper is concentrated at the surface of the SnO_2 agglomerates which have an important influence on the electrical behaviour of polycrystalline films. The same effect of modification of tin dioxide electrical properties by ZnO distributed on the surface of SnO_2 particles has been observed by McAleer *et al.*[14]

The above considerations demonstrate that both bulk doping (for nickel) and surface doping (for copper) give rise to a decrease in the Fermi level and formation of a barrier with activation energy (V) calculated from the relation $R = \exp(V/kT)$.

Taking into account the different distributions of copper and nickel between the bulk and the surface of SnO_2 particles we propose two different mechanisms of interaction with H_2S molecules for SnO_2–CuO and SnO_2–NiO films (Fig. 10). In each several chemical reactions take place simultaneously. According to ref. 15 the reaction resulting in injection of electrons into the depleted surface layer is an interaction of H_2S with O^{2-} ions adsorbed at the SnO_2 surface. In the case of copper, the H_2S molecules react with CuO segregations, producing a transformation of highly resistive CuO to highly conducting CuS. The direct consequence of this reaction is the removal of the p–n junction and an increase in the tin dioxide conductance to the value characteristic for pure tin dioxide. The interaction of H_2S molecules with SnO_2 films doped with nickel involves the following processes: dissociation of H_2S molecules at the surface, diffusion of dissociation products into the bulk and reaction with Ni_{Sn}–O bonds. This interaction gives rise to partial substitution of oxygen atoms by sulfur in the tin dioxide structure and removes the effect of compensation. The more complicated mechanism of H_2S interaction with SnO_2–NiO relative to SnO_2–CuO films and particularly the availability of a slow diffusion process can explain the long response time of films doped with nickel (Fig. 6).

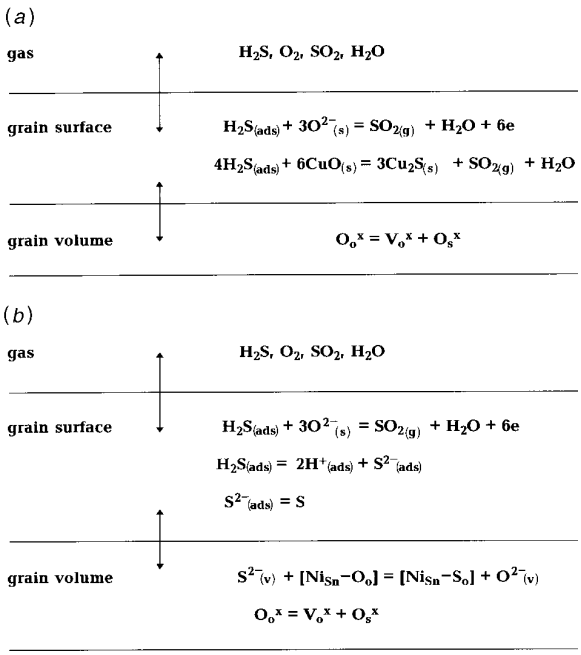

Fig. 10 Model of interaction of SnO_2–CuO (*a*) and SnO_2–NiO (*b*) polycrystalline films with H_2S gas

Conclusions

The pyrosol spraying deposition technique has been used for the synthesis of the SnO_2, SnO_2–CuO and SnO_2–NiO polycrystalline films with average grain size varying from 3 to 10 nm. AES and XPS techniques have demonstrated the different distributions of copper and nickel between the surface and bulk of SnO_2 crystallites.

The effect of additive metals on the electrical properties of tin dioxide films has been investigated. The low-temperature conductivity for Cu- and Ni-doped tin dioxide films shows similar exponential character. This similarity suggests that copper and nickel give rise to barrier formation and as a result enhances significantly the semiconductor resistance. It is proposed that an effect of compensation of V_O^{2+} centres by substitution centres Ni_{Sn}^{2-} has a dominant role in barrier formation for SnO_2 films doped with nickel. By contrast, for films doped with copper it most likely that p–n junctions form at the surface of SnO_2 aggregates.

It is proposed that different impurity locations in nanocrystalline SnO_2 system: nickel in the bulk and copper at the surface, are responsible for the significantly different dynamic sensor properties of the doped films to H_2S detection.

References

1 G. Sberveglieri, S. Groppelli, P. Nelli, C. Perego, G. Valdre and A. Camanzi, *Sens. Actuators B*, 1993, **15–16**, 86.
2 V. Lantto, P. Romppainen, T. S. Rantala and S. Leppavuori, *Sens. Actuators B*, 1991, **4**, 451.
3 K. Takahata, in *Chemical Sensor Technology*, ed. T. Seiyama Kodanska, Tokyo, Elsevier, Amsterdam, 1988, vol. 1, p.39.
4 T. Maekawa, J. Tamaki, N. Miura and N. Yamazoe, *Chem. Lett.*, 1991, **4**, 575.
5 J. Tamaki, T. Maekawa, N. Miura and N. Yamazoe, *Sens. Actuators B*, 1992, **9**, 197.
6 S. Manorama, G. Sarala Devi and V. J. Rao, *Appl. Phys. Lett.*, 1994, **64**, 3163.
7 M. N. Rumyantseva, M. Labeau, J. P. Senateur, G. Delabouglise, M. N. Boulova and A. M. Gaskov, *Mater. Sci. Eng. B*, 1996, **41**, 228.
8 W. R. Smith and R. L. Missen, *Chemical Reaction Equilibrium Analysis: Theory and Algorithms*, John Wiley and Sons, New York, 1982, p. 364.
9 M. N. Rumyantseva, A. M. Gaskov, L. I. Ryabova, J. P. Senateur, B. Chenevier and M. Labeau, *Mater. Sci. Eng. B*, 1996, **41**, 333.
10 J. L. Pouchou and F. Pichoir, *Rech. Aerosp.*, 1984, **N5**, 349.
11 D. E. Ramaker, *J. Electron Spectrosc. Relat. Phenom.*, 1994, **66**, 269.
12 J. Muzusaki, H. Koinuma, J. L. Shimoyama, M. Kawasaki and K. Fueki, *J. Solid State Chem.*, 1990, **8**, 443.
13 H. Takayasu, *Fractals in the Physical Science*, Manchester University Press, Manchester and New York, 168 p.
14 J. F. McAleer, P. T. Moseley, J. O. W. Norris, D. E. Williams and B. C. Tofield, *J. Chem. Soc., Faraday Trans. 1*, 1988, **84**, 441.
15 J. N. Zemel, *Thin Solid Films*, 1988, **163**, 189.

Paper 7/01896G; *Received* 18*th March*, 1997